Electronic Supplementary Material (ESI) for Sustainable Energy & Fuels.
This journal is © The Royal Society of Chemistry 2021

Supporting Information

Fast and Scaled-up Synthesis of Amorphous C,N co-doped Mesoporous Co-based Phosphates as Advanced Electrodes for Supercapacitors and Water Oxidation

Zheng-Han Guo,[a] Jie-Ying Lin,[a] Pei-Ru Chen,[a] Kai-Qin Ou,[a] Xiang-Ya Xu,[b] Jin-Kun Li,[a] Sai Huang,[a] Xin-Xin Sang,[a] Jing-Chen Liu [a] and Jun-Ling Song[a]*

Table of Content

Experimental Section

R_s and R_{ct} of all prepared catalysts……Table S1

Performance comparison between C*x*NCPO-450 and other reported OER catalysts…….……..…Table S2

Performance comparison between C4NCPO and C4NCPO-450 and other reported materials for Supercapacitor……..…Table S3

The output of C4NCPO synthesized at one time (a); (b) C4NCPO prepared by expanding the base of raw materials.……Figure. S1

TGA curves of (a) C3NCPO; (c) C4NCPO; (e) C6NCPO and PXRD patterns of (b) C3NCPO-y; (d) C4NCPO-y; (f) C6NCPO-y.…….…….……Figure. S2

Charge-to-mass (m/z) ratio measured by TGA-MS…….…..…Figure. S3

FTIR of (a) C*x*NCPO and (a) C*x*NCPO-450….…….…….……Figure. S4

Raman spectroscopy of (a) C3NCPO-y; (b) C4NCPO-y; (c) C6NCPO-y.……Figure.S5

EPR analysis of C4NCPO and C*x*NCPO-450……Figure. S6

The conductivity of C*x*NCPO-450 measured with a conductivity meter using the four-probe method……Figure. S7

SEM images of (a) C3NCPO; (b) C3NCPO-400; (c) C3NCPO-450; (d) C3NCPO-550; (e) C3NCPO-650…….……Figure. S8

SEM images of (a) C4NCPO; (b) C4NCPO-400; (c) C4NCPO-450; (d) C4NCPO-550…….……. Figure. S9

SEM images of (a) C6NCPO; (b) C6NCPO-350; (c) C6NCPO-400; (d) C6NCPO-450; (e) C6NCPO-550……. Figure. S10

Corresponding pore size distribution from BET……. Figure. S11

LSV curve of C3NCPO-y(a), C4NCPO-y(d), C6NCPO-y(h); Corresponding Tafel slope(b)(e)(h) and Comparison of overpotential and Tafel slope (c)(f)(i) (error bar shows the error of several measurements) ……. Figure. S12

Cyclic voltammograms of (a) C3NCPO; (b) C3NCPO -400; (c) C3NCPO -450; (d) C3NCPO -550 at different scan rates from 20 to 100 mV s^{-1}. …… Figure. S13

Cyclic voltammograms of (a) C4NCPO; (b) C4NCPO -400; (c) C4NCPO -450; (d) C4NCPO -550 at different scan rates from 20 to 100 mV s^{-1} ...……Figure. S14

Cyclic voltammograms of (a) C6NCPO; (b) C6NCPO -350; (c) C6NCPO -400; (d) C6NCPO-450; (e) C6NCPO-550 at different scan rates from 20 to 100 mV……Figure. S15

Plots of the currentdensity at 1.14 V vs. the scan rate（20 mV s^{-1}, 40 mV s^{-1}, 60 mV s^{-1}, 80 mV s^{-1}, 100 mV s^{-1}) for C3NCPO-y(a), C4NCPO-y(b), C6NCPO-y(c) ……Figure. S16

Nyquist plots of C3NCPO-y(a), C4NCPO-y(b), C6NCPO-y(c), inset: equivalent circuit ……Figure. S17

Original and fitted EIS diagrams of IrO_2, C4NCPO, C4NCPO-450……Figure. S18

(a) The linear relationship between oxygen concentration and oxygen chromatographic peak area; (b) The relationship between experimental and theoretical oxygen production and time; (c) Chronopotentiometry curve of CNCP-450 at voltage of 1.50 V *vs*. RHE loaded on carbon cloth. ……Figure. S19

XRD (a), SEM (b) and XPS (c-h) of C4NCPO-450 after 2000 CV ……Figure. S20

The galvanostatic charge–discharge curves (GCD) at different current densities of C4NCPO ……Figure. S21

SEM images of CNCPO-450 after charging and discharging cycles (a) and corresponding SEM-mapping(b)…….....Figure. S22

XRD patterns after C4NCPO-450 charge and discharge cycle……Figure. S23

Three consecutive measurements of the specific capacitance of C4NCPO-450.. …… Figure S24.

Experimental Section

Reagents and materials: All reagents used in this study were purchased and directly used without further purification. KOH (99.0%) were purchased from Sinopharm Chemical Reagent. $CoCl_2$(AR), 1,3-propanediamine (AR), 1,4-butanediamine (AR), 1,6-Hexanediamine (AR), phosphoric acid (85%, GR), IrO_2 (99.95%) and ethylene glycol were obtained from Admas-beta, perfluorosulfonic acid−poly-(tetrafluoroethylene) copolymer (Nafion solution, 5% w/w in water) were purchased from Alfa-Aear.

Physical characterizations: The structure of C*x*NCPO-y is determined by PXRD (Bruker D8, Cu-Kα). the spectra were recorded in the 2θ range of 5° to 50°. The morphology of C*x*NCPO and C*x*NCPO-y were investigated by scanning electron microscopy (SEM, Hitach S-4800) and transmission electron microscope (TEM, JEOL 2100F). X-ray electron spectroscopy (XPS) was performed on PHI 5000 Versaprobe III. All spectra were calibrated by C 1s (284.8 eV). TGA-MS (Thermo plus EVO2) analysis was carried out in the range of 50-900°C at a heating rate of 10°/min under N_2 atmosphere to dynamically detect the gas generated by annealing. The Raman spectra of C*x*NCPO-y were collected with a Raman spectrometer (inVia, United Kingdom) using a 532 nm laser. FT-IR spectra were collected using Fourier transform infrared spectrometer (FTIR, Nicolet 6700). The N_2 adsorption and desorption curve was

measured on the Brunauer-Emmett-Teller (BET, ASAP2020 MP). Element analyzer (EA, Vario EL Cube) was used to quantitatively analyze the content of C and N in materials. An electron paramagnetic resonance spectrometer (EPR, Bruker A300) was used for electron spin resonance (ESR) measurements. The conductivity is measured by the four-probe method of the conductivity meter (ST2722SD+ST2643) after pressing the powder sample.

OER performance test: All electrochemical tests were carried out in a three-electrode system using a CHI760E electrochemical workstation (Shanghai Chenhua, China). Pt wire and Hg/HgO were used as counter electrode and reference electrode, respectively. The glassy carbon electrode (GC) loaded with the prepared catalyst was used as the working electrode (surface area = 0.07 cm^2). 5mg of the above prepared catalyst was added into 1 mL solution of ethanol and water (1:1, v/v), and then adding 10 μL nafion (5.0 wt %) to the above mixture, and this suspension was uniformly dispersed by ultrasonical-method. Before the electrochemical test, the 1.0 M KOH solution was bubbled with O_2 for at least 30 mins to reach the H_2O/O_2 equilibrium at room temperature. Besides cyclic voltammetry (CV) was applied to make the electrode reach a steady state at a sweep rate of 100 mV/s before LSV test. The measured voltage value is converted into the electrode potential vs the reversible hydrogen electrode by the equation $E_{RHE}=E_{Hg/HgO}+ 0.059\ pH+0.098\ V$. Electrochemical impedance spectroscopy (EIS) measurements were recorded in the frequency range of 10^5–0.1 Hz with an amplitude of 5 mV. The electric double layer capacitance of the prepared catalyst was

determined by the CV of different scanning speeds (20, 40, 60, 80, 100 mV s^{-1}) in without-iR compensation has not been applied to this work.

Super capacitor performance test: All tests are carried out in 3 M KOH, typically, Pt plate is the counter electrode and Hg/HgO is the reference electrode. The active electrode material including catalyst, acetylene black and polytetrafluoroethylene (PVDF) (mass ratio 8:1:1) was mixed and dispersed in 1 mL ethanol ultrasonically until the mixture is uniform. After that, an amount of slurry was doped on 1 cm × 2 cm foam nickel (NF) and the coating size is about 1 cm × 1cm. The foam nickel loaded with the active material was dried overnight at 60 ℃, then, the dried foam nickel was pressed into a tablet under a pressure of 5.0 MPa using a tablet press. The above pressed NF loaded with active material was used as the positive electrode. The specific capacitance of the material is calculated according to the mass method.

$$m = m2 - m1 \qquad (1)$$

among them, *m2* represents the mass of NF loaded with active substance after compression, *m1* refers to the mass of blank NF.

Cyclic voltammetry (CV) and galvanostatic charge–discharge (GCD) were carried out on an electrochemical workstation (CH1760E, Chenhua, China). Then, the specific capacitance (C, F g^{-1}), energy density (E, Wh kg^{-1}) and power density (P, W kg^{-1}) were calculated according to the following equations:

$$C = \frac{I\Delta t}{m\Delta V} \qquad (2)$$

$$E = \frac{1}{2}C\Delta V^2 \qquad (3)$$

$$P = \frac{3600E}{\Delta t} \qquad (4)$$

where I(A), Δt (s), m(g) and ΔV (V) represent the charge current, discharge time, mass of active materials and potential window, respectively.

Calculation Method:

The values of mass activity (A g^{-1}) were calculated from the catalyst loading m (0.03 mg cm^{-2}) and the measured current density j (mA cm^{-2}) at η = 0.35 V:

The values of TOF were calculated by assuming that every metal atom is involved in the catalysis (lower TOF limits were calculated):

$$\mathrm{TOF} = \frac{j \cdot S_{\mathrm{geo}}}{4F \cdot n}$$

Here, j (mA cm^{-2}) is the measured current density at η = 0.35 V, S_{geo} (0.07 cm^2) is the surface area of glassy carbon disk, the number 4 means 4 electrons per mole of O_2, F is Faraday's constant (96485.3 C mol^{-1}), and n is the moles of the metal atom on the electrode calculated from m and the molecular weight of the coated catalysts.

The turnover frequency (TOF) of the catalyst for OER is defined as TOF = $n$$O_2$/$n$cat/$t$ where $n$$O_2$ is the amount of oxygen (mol) produced, $n$cat is the amount of catalytic active centers in the catalyst (mol) and t is the electrolysis time (s).

When the electrolysis current is all used for OER,

$$\mathrm{TOF}_{\mathrm{theoretical}} = J/(4\times F\times m/\mathrm{M})$$

Where J is the current density (mA cm^{-2}) at a given overpotential, F is the faraday constant (96485 C mol^{-1}), m is the mass loading of the catalyst (mg cm^{-2}), and M is the molecular weight of the catalyst unified with one active center per formula unit.

The Faraday efficiency for OER (F_{OER}) is calculated by

$$F_{\mathrm{OER}} = \mathrm{TOF} / \mathrm{TOF}_{\mathrm{theoretical}} \times 100\%$$

	0min	5min	10min	15min	20min	25min
O_2	537076.5	553990.9	571041.8	586538.5	601110.1	616297.9
N_2	1883965.2	1965004.1	2041021.0	2091701.9	2159922.9	2172776.2
H_2	/	14530.1	20421.4	22500.1	31117.2	35549.1

Pour N_2 into 1 M KOH solution to saturation before testing, the peak areas of O_2, N_2 and H_2 determined by gas chromatography are shown in the table below:

Giving nO_2 = O_2 concentration (%) × head space volume / (22.4 × 288/ 273);

ncat = mass loading (mg) / molecular weight / 1000

TOF = n_{O2}/ ncat / 300;

Considering all Co ions in C4NCPO-450 as catalytic centers. $TOF_{Theoretical}$ = 10.0 / (4 × 96485 × mass loading (mg) / molecular weight).

The catalyst loading is 0.03 mg cm^{-2} and the current density is 10 mA cm^{-2}, take 0-5 min as an example:

n_{O2}= (553990.9 -537076.5)/ (2993805) ×32/ (1000×22.4×298/273)

=7.39× 10^{-6}

ncat= 0.03/ (200× 81% ×1000) =1.85× 10^{-7}

TOF= n_{O2}/ ncat=7.39× 10^{-6}/1.85× 10^{-7}/300=0.133 s^{-1}

TOF theoretical =10/ (4×96485×0.03/200× 81%) = 0.14 s^{-1}

F_{OER} = TOF/ TOF theoretical=0.133/0.14= 95.0 %

Table S1. R_s and R_{ct} of all prepared catalysts.

	IrO_2	C3NCPO	C3NCPO-450	C4NCPO	C4NCPO-450	C6NCPO	C6NCPO-450
R_s	0.53	7.25	7.56	5.65	7.65	7.22	8.75
R_{ct}	7.9	8.45	2.97	2.00	0.32	2.97	1.90

Table S2. Performance comparison between C*x*NCPO-450 and other reported OER catalysts.

Catalyst	Electrolyte	Substrate	Overpotential at 10 mA/cm^2 (mV vs.RHE)	Tafel slope (mV dec^{-1})	Reference
C3NCPO-450	**1.0 M KOH**	**GC**	**296**	**75.01**	**This work**
C4NCPO-450	**1.0 M KOH**	**GC**	**292**	**67.45**	**This work**
C6NCPO-450	**1.0 M KOH**	**GC**	**296**	**75.98**	**This work**
$Fe_{0.43}Co_{2.57}(PO_4)_2$/Cu	1.0 M KOH	Cu wire	310	40.2	*ACS Sustainable Chem. Eng*. **2020**, 8, 36, 13793–13804
$Fe_{2.95}(PO_4)_2(OH)_2$	1.0 M KOH	GC	281	/	*Electrochimica Acta*. **2019**,319,118-128.
Sn-FeHP	1.0 M	GC	359	91	*Catal. Sci. Technol*,

	KOH				**2017**, 7, 5092
$Co_3(PO_4)_2$-Co_3O_4	1.0 M KOH	GC	270	39	*Small*. **2017**, 13, 1701875
$Ni_{12}P_5/Ni_3(PO_4)_2$	1.0 M KOH	GC	318	51.7	*Appl. Catal. B: Environ*, **2017**,204, 486–496
$Co_3(PO_4)_2$@N-C	1.0 M KOH	GC	317	62	*J. Mater. Chem. A*. 2016, 4, 8155
Ni-Co phosphate	1.0 M KOH	GC	310	68	*Chem.Mater*. **2020**, 32, 7005−7018.
$Co_7(PO_4)_2(HPO_4)_4$	1.0 M KOH	GC	293	40.63	*Electrochimica Acta.* **2020**,337,135827.
NiCo-2.0-800HP	1.0 M KOH	GC	320	84	*J.Mater.Chem.A.***2020**, 8,3035-3047.
IrO_2	1.0 M KOH	GC	305	79.32	*This work*
IrO_2	1.0 M KOH	GC	301	74.8	*Chem.Eng.J.**2020**,399, 125799.*
IrO_2	1.0 M KOH	GC	320	75.39	*J.Power.Sources.2021, 498,229859.*

Table S3. Performance comparison between C4NCPO and C4NCPO-450 and other reported materials for Supercapacitor.

Material	Synthesis method	Electrolyte	Specific capacitance	Stability	Reference
C4NCPO	Hydrothermal	3.0 M KOH	104 F g^{-1}@1 A g^{-1}	/	**This work**
C4NCPO-	Hydrothermal	3.0 M	326 F g^{-1}@1 A g^{-1}	2200 cycles @	**This work**

450		KOH		82.4%	
$Co_{11}(HPO_3)_8(OH)_6$	Hydrothermal	3M KOH	312 F g^{-1}@1.5A g^{-1}	2200 cycles @ 89.4%	*Nanoscale*.**2013**, 5,503-507
$Co_7(PO_4)_2(HPO_4)_4$-NMP	Solvothermal	3M KOH	345 F g^{-1} @ 1 A g^{-1}	2000 cycles @ 80.14%	*Electrochimica Acta.* **2020**,337,135827 .
Si-C	Solvothermal followed by annealing	1M KOH	254.0 F g^{-1} @ 0.2 A g^{-1}	3000 cycles @ 97%	*Electrochimica Acta* **2021**,370, 137813.
$Ni_{11}(HPO_3)_8(OH)_6$	Hydrothermal	3M KOH	295.0 F g^{-1} @ 0.625 A g^{-1}	1000 cycles @ 99.3%	*Part. Part. Syst. Charact.***2013**,30, 287-298
$Co_3(PO_4)8H_2O$	Green precipitate process	3M KOH	350 F g^{-1} @ 1 A g^{-1}	1000 cycles @ 102%	*Matter. Lett.* ***2015,*** 152,25-28.
CNPO-40//BPO	Solvothermal	3M KOH	264.3 F g^{-1} @ 1 A g^{-1}	10000 cycles@ 93.03%	*ACS. Appl. Mater. Inter.*DOI: 10.1021/acsami.1c04614
Mn3O4@NPC	Annel-hydrothermal	1M Na_2SO_4	370.8 F g^{-1} @ 1 A g^{-1}	10000 cycles@ 95.68%	*Chem. Eur. J.* ***2021,*** 407, 126874.
$NH_4(NiCo)PO4{\cdot}H_2O$/GF	Hydrothermal	3M KOH	111 mAh g^{-1} @ 0.5 A g^{-1}	10000 cycles@ 70%	*J. Alloy. Compd.* ***2021***, 883, 160897.
NCoHPOF-450	Ionic liquid	3M KOH	206 F g-1 @ 1 A g-1	3000 cycles @ 80%	*Chem. Eur. J. 2021, 27, 7731–*

7737.

(PANI/PBF-NPs	hydrothermal	3M KOH	225 F g^{-1} @ 0.9 A g^{-1}	1000 cycles @ 94%	*Int. J. Hydrog. Energy.* ***2019****, 44, 28088.*
Mo–NiS_2@NiCo-LDH	hydrothermal	6M KOH	325.6 mAh g^{-1} @ 1 A g^{-1}	3000 cycles @ ~98%	*J. Power Sources.* ***2021****, 509, 230333.*
$Mn_3(PO_4)_2$/GF	hydrothermal	3M KOH	270 F g^{-1}(0.5 A g^{-1})	10000 cycles @ ~96%	*J. Colloid Interface Sci.* ***2017****, 494, 325.*

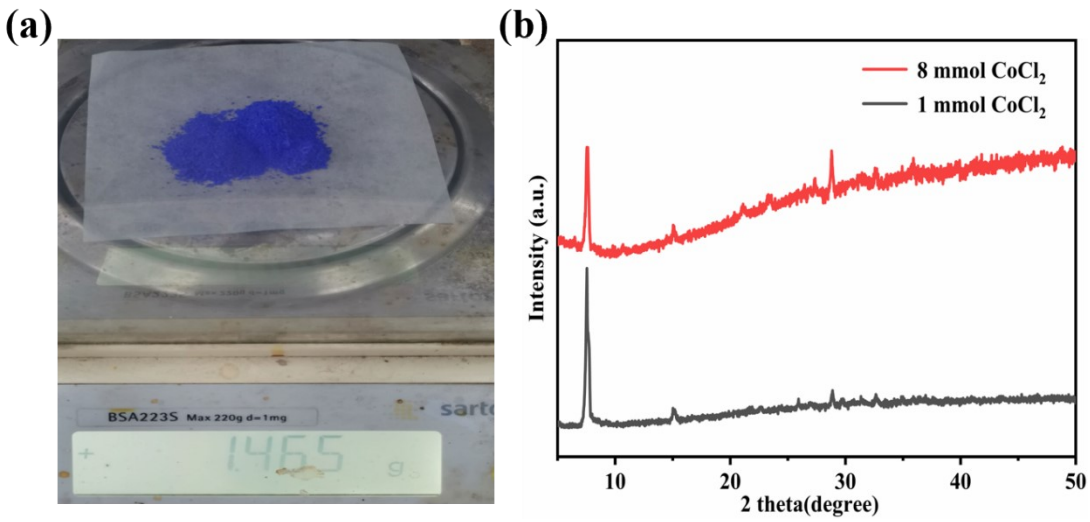

Figure. S1. (a) The output of C4NCPO synthesized at one time; (b) C4NCPO prepared by expanding the base of raw materials.

Note: Yield=1.465/200/8=91.6%, based on the molar amount of Co. Among them, the relative molecular mass of C4NCPO is 200 g/mol.

Experimental part: 8 mmol $CoCl_2$, 2 mL H_3PO_4, and 12 mL H_2O, 12 mL ethylene glycol were mixed, then 6 mL 1,4-butanediamine was added, the mixture was transferred to a high-pressure tube, react at 150 ℃ for 1 h at 900 rpm. The sample was washed at least three times with water and ethanol to obtain the product.

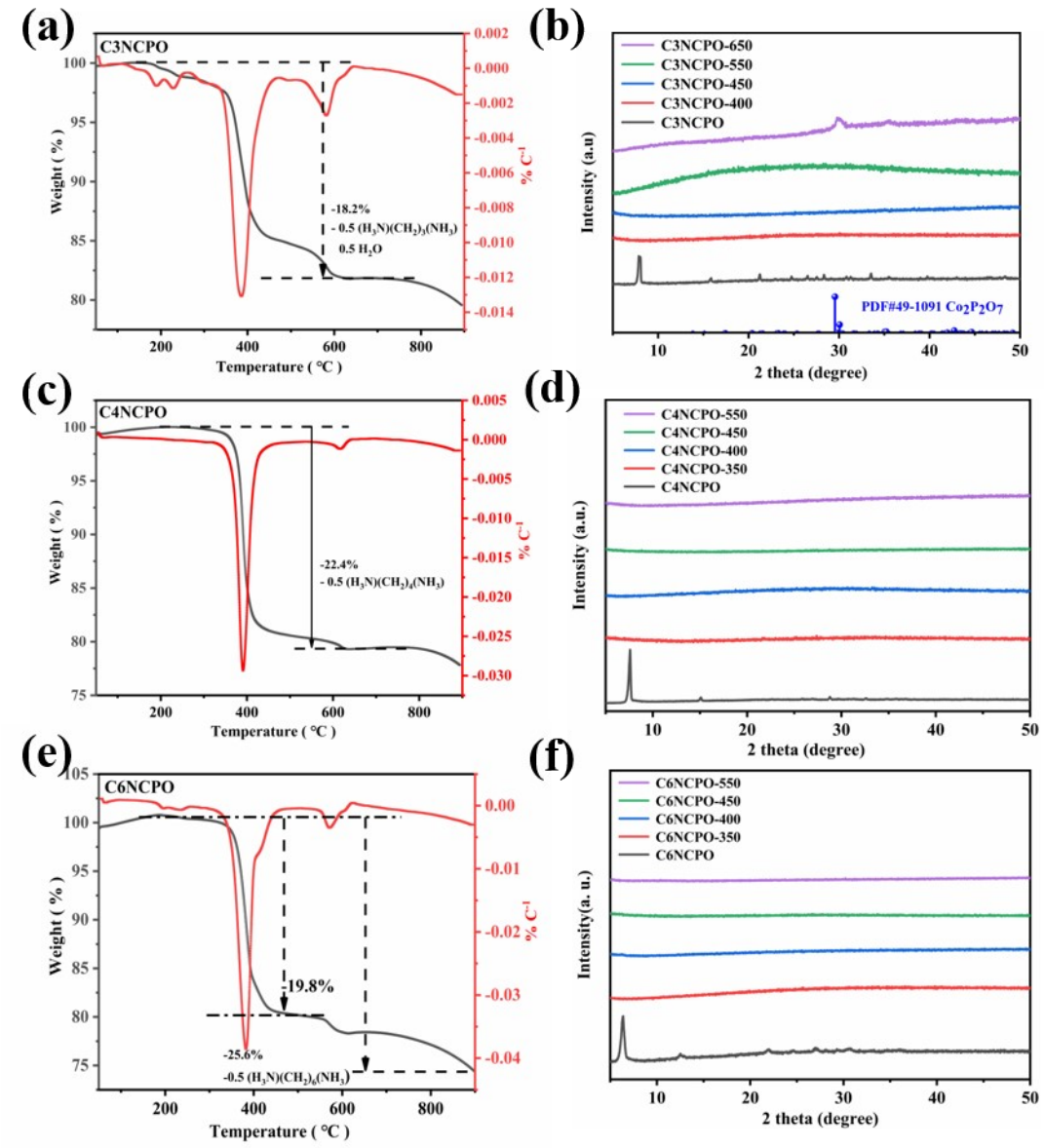

Figure. S2. TGA curves of (a) C3NCPO; (c) C4NCPO; (e) C6NCPO and PXRD patterns of (b) C3NCPO-y; (d) C4NCPO-y; (f) C6NCPO-y.

Note: When calculating the molecular weight, C4NCPO and C6NCPO have not crystalline water. For C3NCPO, C4NCPO and C6NCPO, their thermogravimetric investigation (TGA) uncovers two primary phases of weight reduction. First, a major weight loss of 18.2% for C3NCPO, 22.4% for C4NCPO and 25.6% for C6NCPO was observed from 200-600 ºC due to decomposition of precursors. Especially, for C6NCPO, when the temperature reaches 450°C, the weight loss is 19.8%, indicating the precursor with longer chain length more easily decomposed. And PXRD demonstrated all the calcined products that CxNCP-y (*x*= 3, 4, 6; y=350,400,450 and 550) are amorphous.

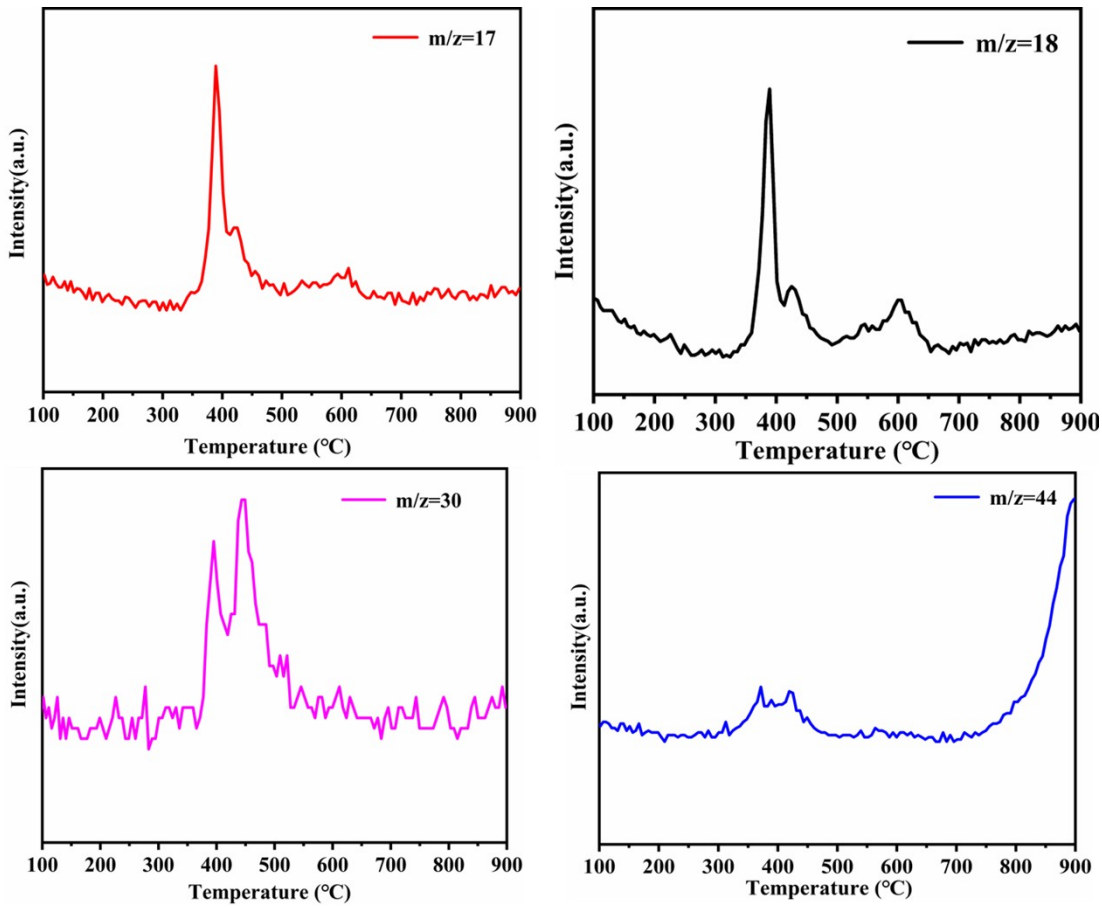

Figure. S3. Charge-to-mass (m/z) ratio measured by TGA-MS.

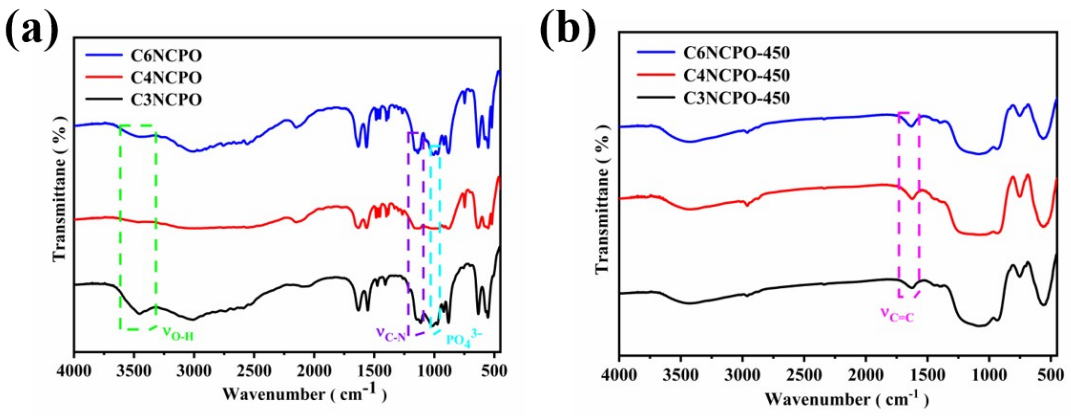

Figure. S4. FTIR of (a) C*x*NCPO and (a) C*x*NCPO-450.

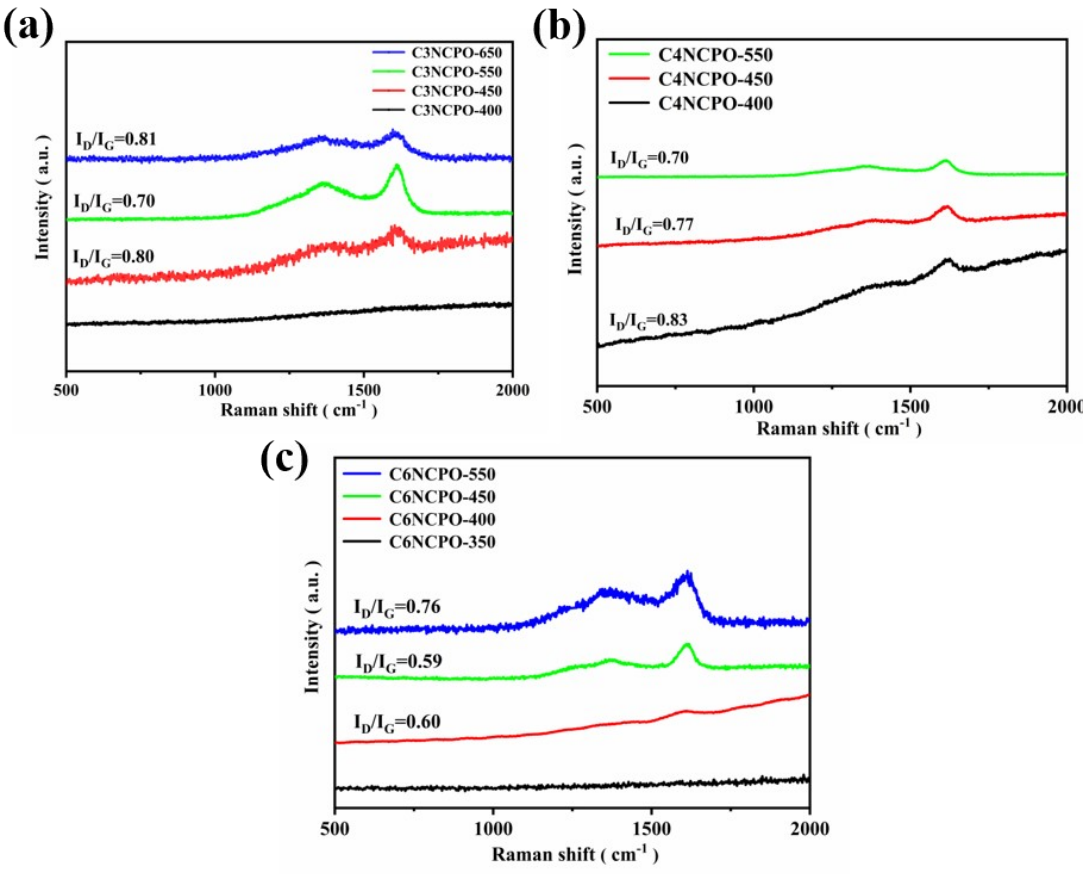

Figure. S5. Raman spectra of (a) C3NCPO-y; (b) C4NCPO-y; (c) C6NCPO-y.

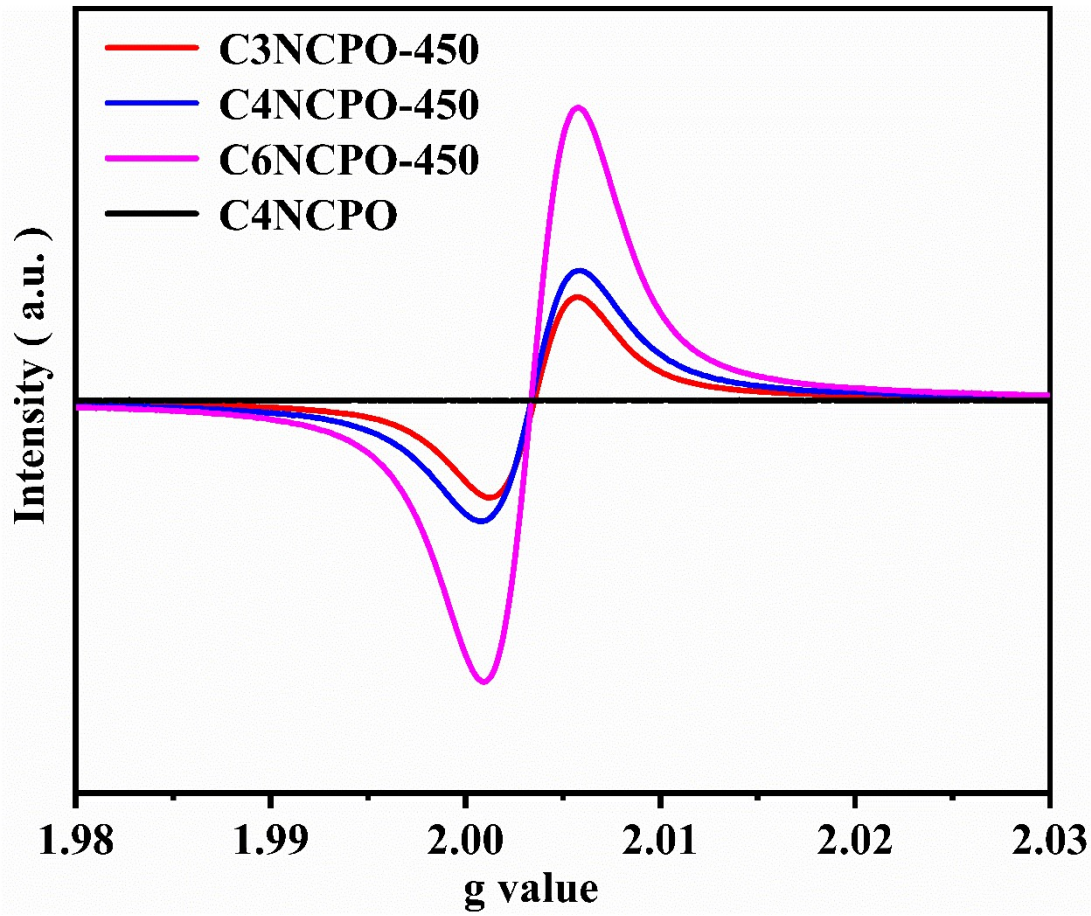

Figure. S6. EPR analysis of C4NCPO and ea.

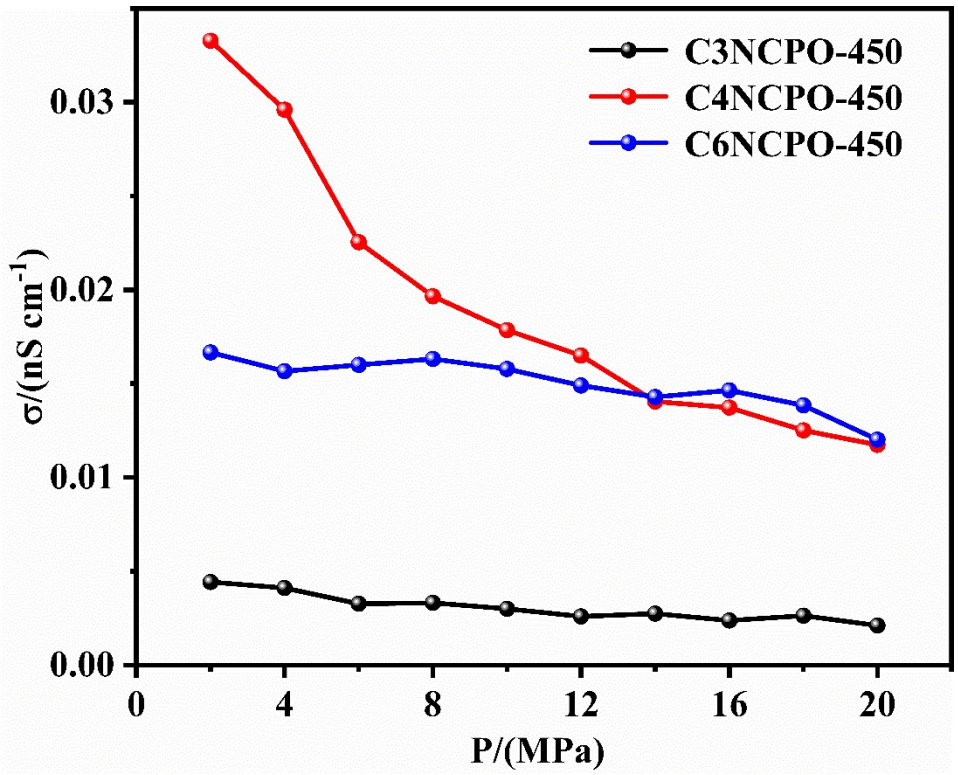

Figure. S7. The conductivity of C*x*NCPO-450 measured with a conductivity meter using the four-probe method.

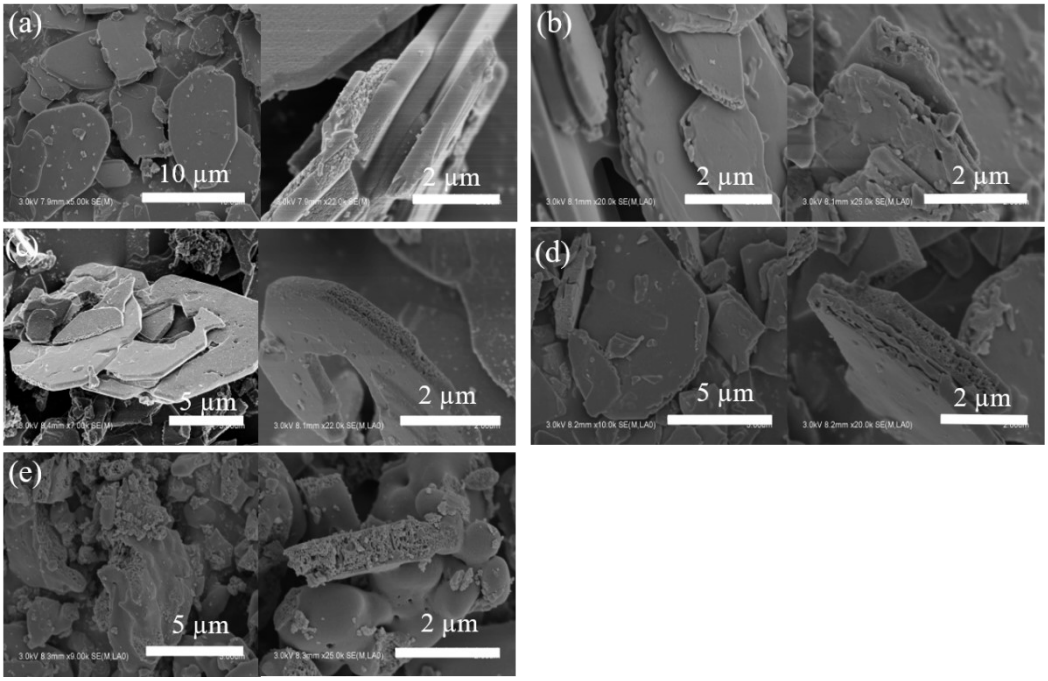

Figure. S8. SEM images of (a) C3NCPO; (b) C3NCPO-400; (c) C3NCPO-450; (d) C3NCPO-550; (e) C3NCPO-650.

Note: Uniform lamellar morphologies could be observed in Fig. S8(a-d). As shown in Fig. S8(e), the samples collapsed, besides, pyrophosphate was formed calcination at 650 ^{o}C according to XRD results.

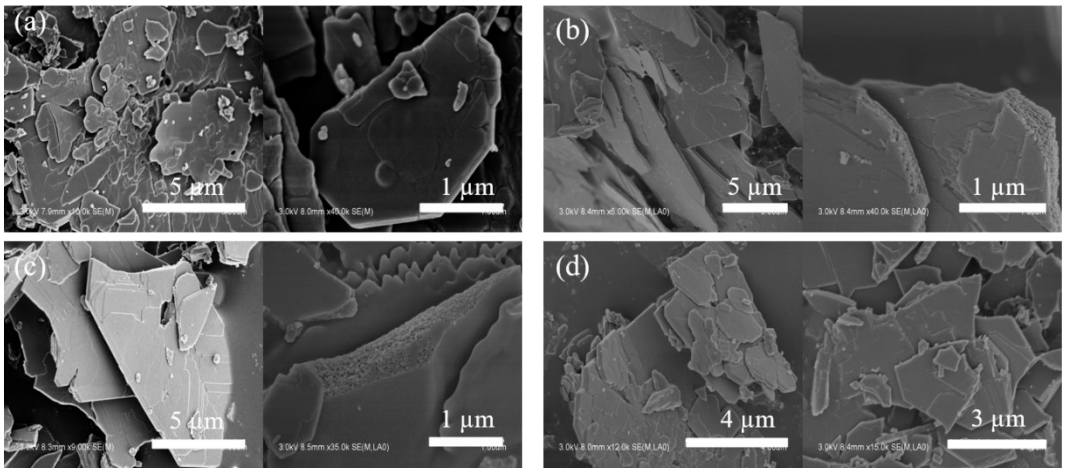

Figure. S9. SEM images of (a) C4NCPO; (b) C4NCPO-400; (c) C4NCPO-450; (d) C4NCPO-550.

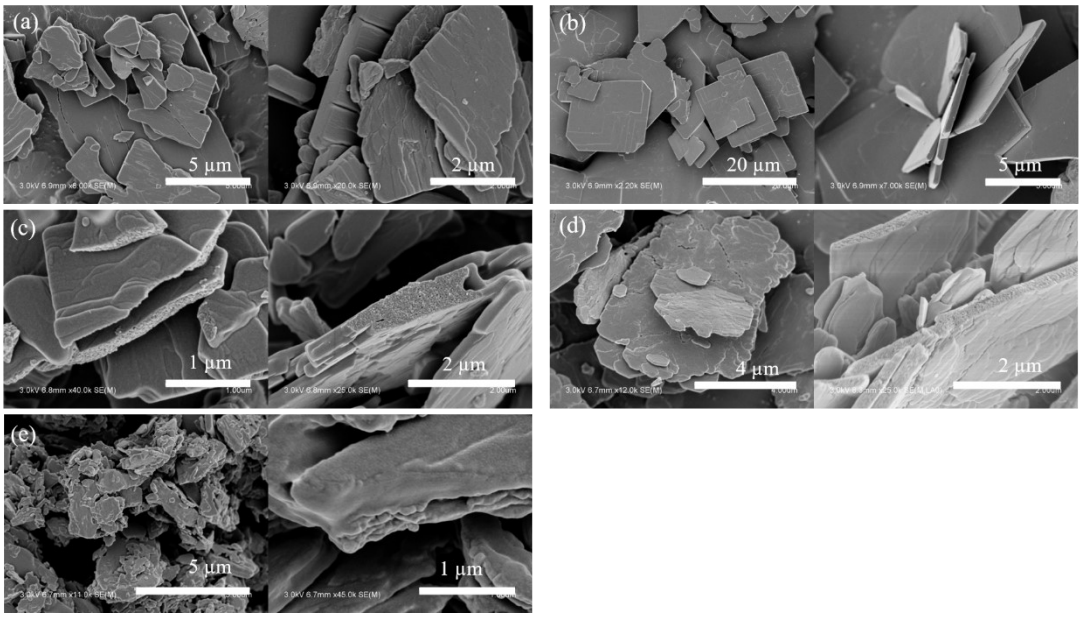

Figure. S10. SEM images of (a) C6NCPO; (b) C6NCPO-350; (c) C6NCPO-400; (d) C6NCPO-450; (e) C6NCPO-550.

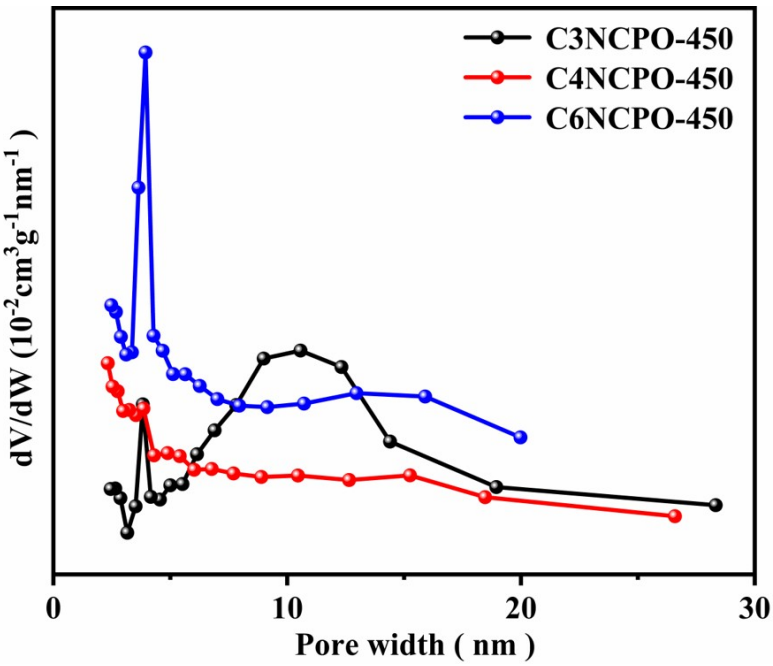

Figure. S11. Corresponding pore size distribution of different calcined samples in this study.

Notes: The BET specific surface areas of C3NCPO-450, C4NCPO-450 and C6NCPO-450 are 2.94 m^2/g, 2.93 m^2/g, and 5.49 m^2/g, respectively.

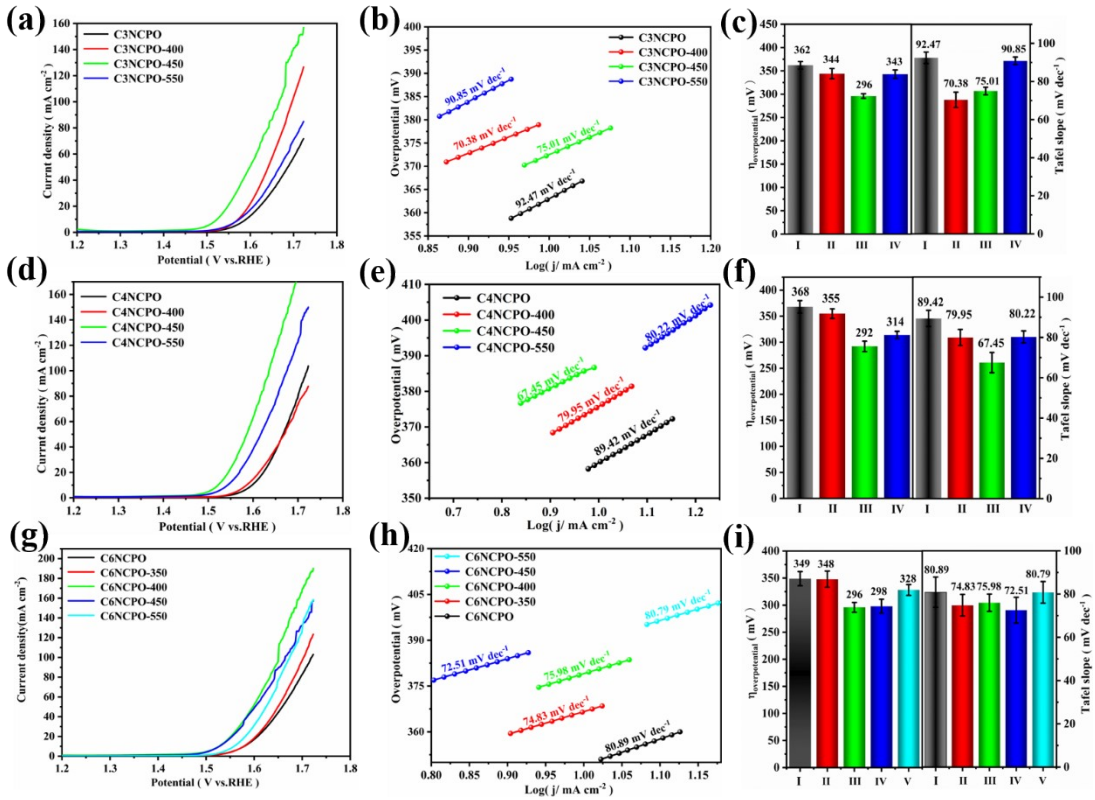

Figure. S12. LSV curve of C3NCPO-y(a), C4NCPO-y(d), C6NCPO-y (h); Corresponding Tafel slope(b)(e)(h) and Comparison of overpotential and Tafel slope (c)(f)(i) (error bar shows the error of several measurements).

Note: (c) I:C3NCPO; II: C3NCPO-400; III: C3NCPO-450; IV: C3NCPO-550; (f) I:C4NCPO; II: C4NCPO-400; III: C4NCPO-450; IV: C4NCPO-550; (i) I:C6NCPO; II: C6NCPO-350; III: C6NCPO-400; IV: C6NCPO-450; V: C6NCPO-550.

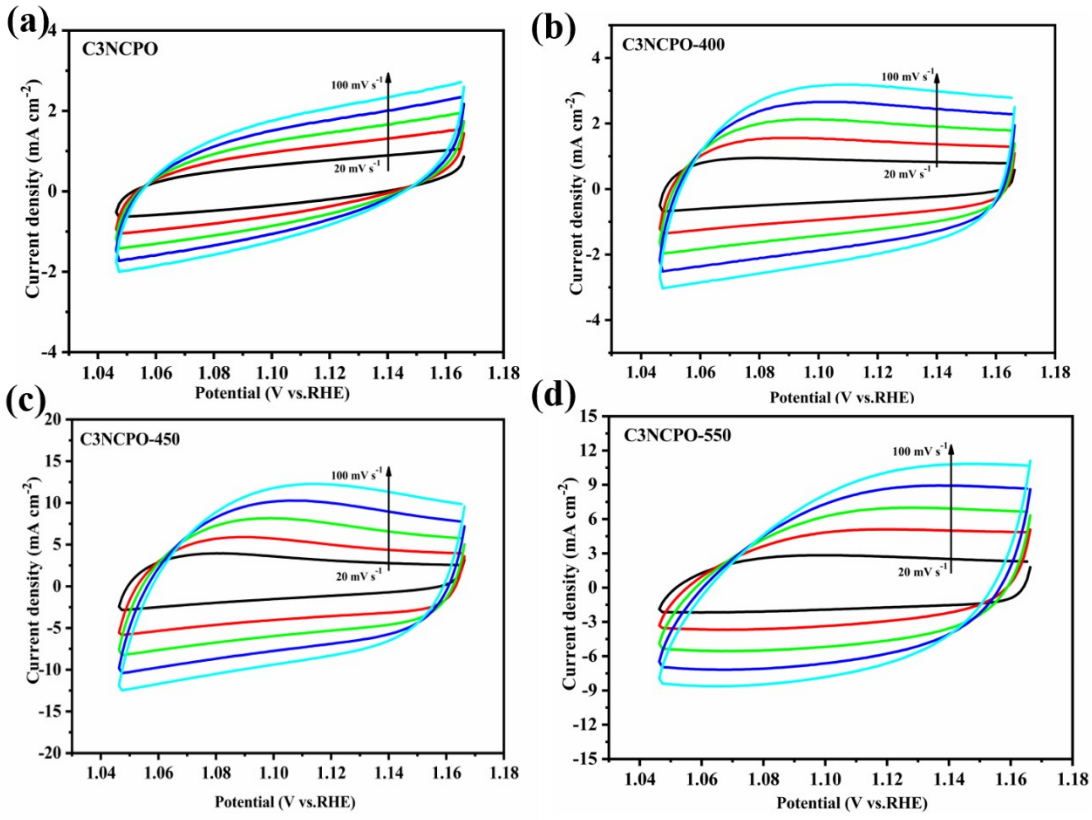

Figure. S13. Cyclic voltammograms of (a) C3NCPO; (b) C3NCPO -400; (c) C3NCPO -450; (d) C3NCPO -550 at different scan rates from 20 to 100 mV s^{-1}.

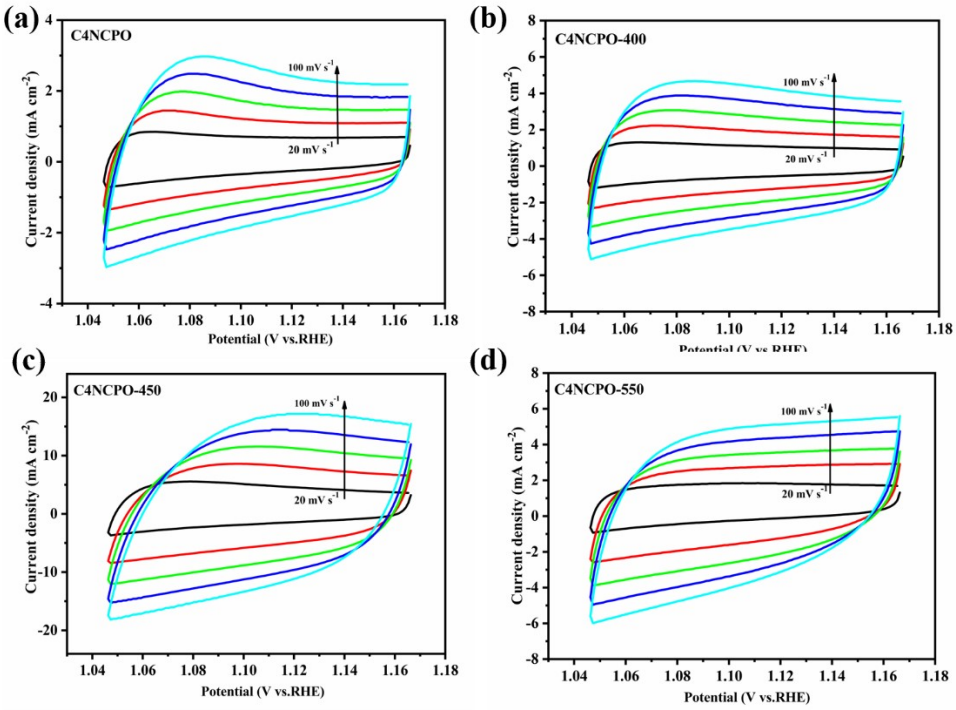

Figure. S14. Cyclic voltammograms of (a) C4NCPO; (b) C4NCPO -400; (c) C4NCPO -450; (d) C4NCPO -550 at different scan rates from 20 to 100 mV s^{-1}.

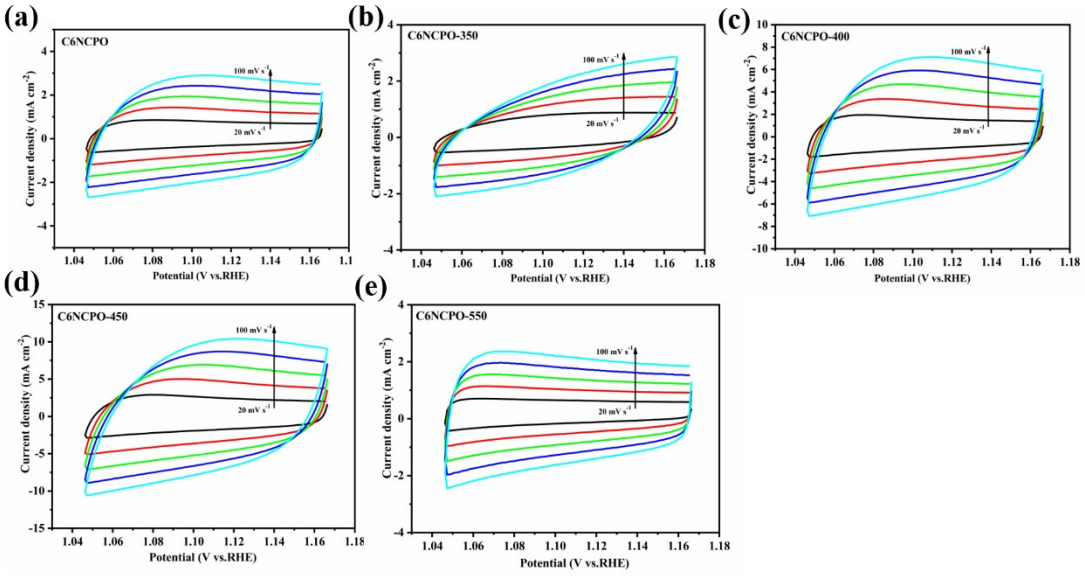

Figure. S15. Cyclic voltammograms of (a) C6NCPO; (b) C6NCPO -350; (c) C6NCPO -400; (d) C6NCPO -450; (e) C6NCPO -550 at different scan rates from 20 to 100 mV s^{-1}.

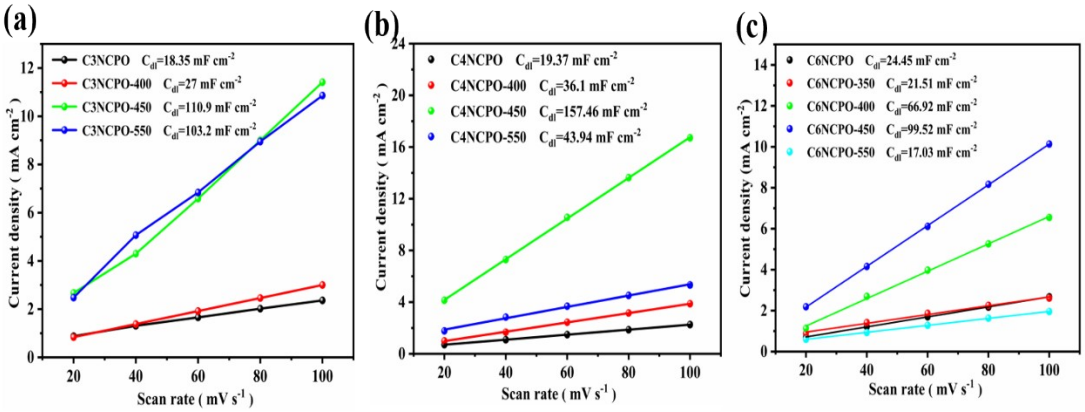

Figure. 16. Plots of the currentdensity at 1.14 V vs. the scan rate（20 mV s^{-1}, 40 mV s^{-1}, 60 mV s^{-1}, 80 mV s^{-1}, 100 mV s^{-1}) for C3NCPO-y(a), C4NCPO-y(b), C6NCPO-y(c).

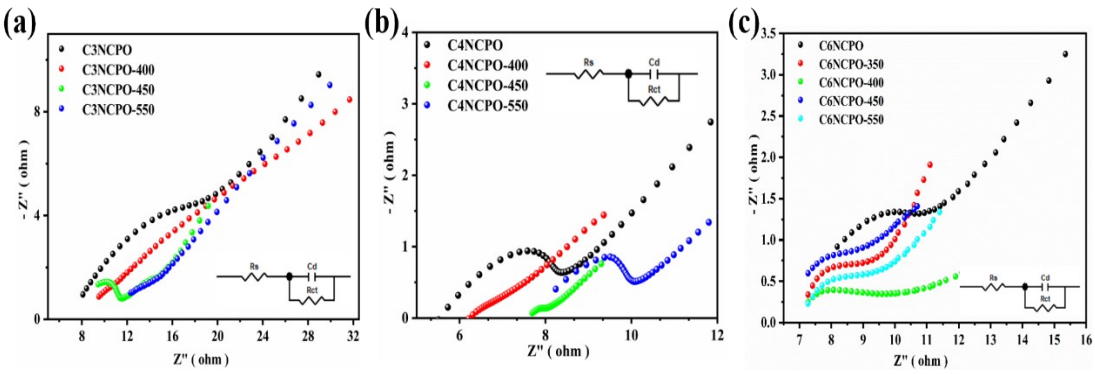

Figure. S17. Nyquist plots of C3NCPO-y(a), C4NCPO-y(b), C6NCPO-y(c), inset: equivalent circuit.

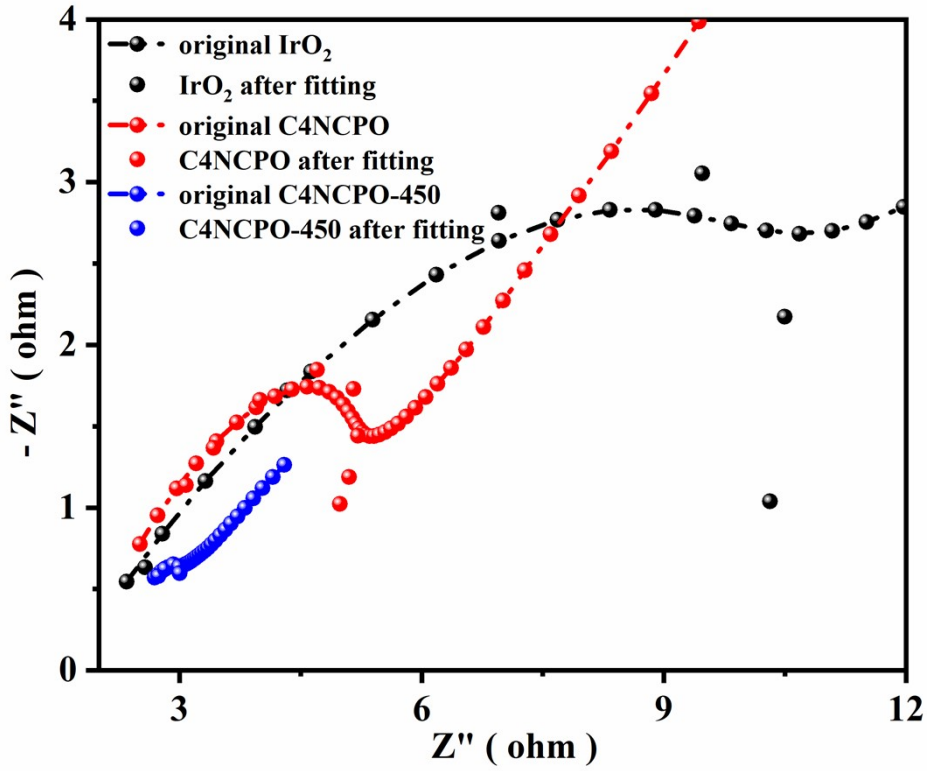

Figure. S18. Original and fitted EIS diagrams of IrO_2, C4NCPO, C4NCPO-450.

Note: The Rs and Rct values of IrO_2, C4NCPO, and C4NCPO-450 in the text are obtained by curve fitting.

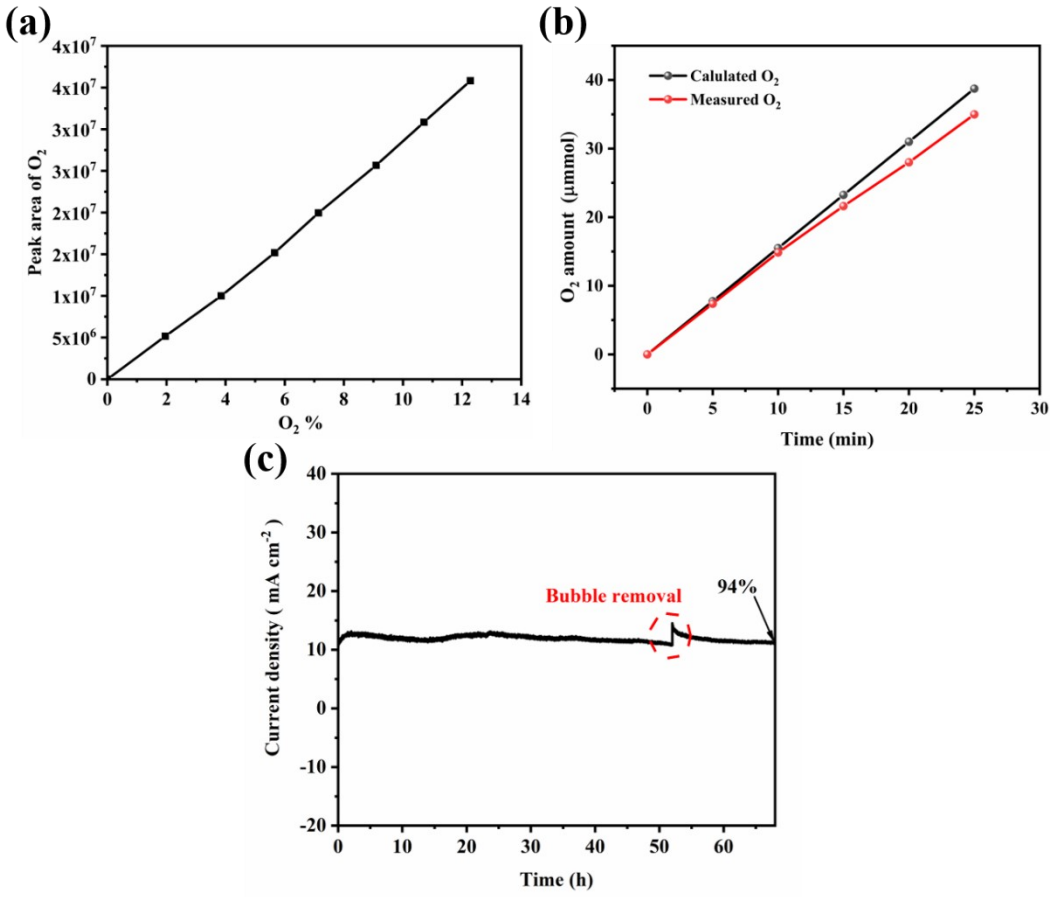

Figure. S19. (a) The linear relationship between oxygen concentration and oxygen chromatographic peak area; (b) The relationship between experimental and theoretical oxygen production and time; (c) Chronopotentiometry curve of C4NCPO-450 loaded on carbon cloth at voltage of 1.50 V *vs*. RHE.

Note: In the calculation method section, an example of FE calculation within 0-5min has been given. Because the bubble is adsorbed on the GC, the oxygen production will be low in some time periods. Therefore, the slope by fitting the Faraday efficiency from five points, compare with standard standard curve line, FE=90%. For Figure S19c, the fluctuation of the curve should be caused by the removal of bubbles adsorbed on the electrode during continuous testing.

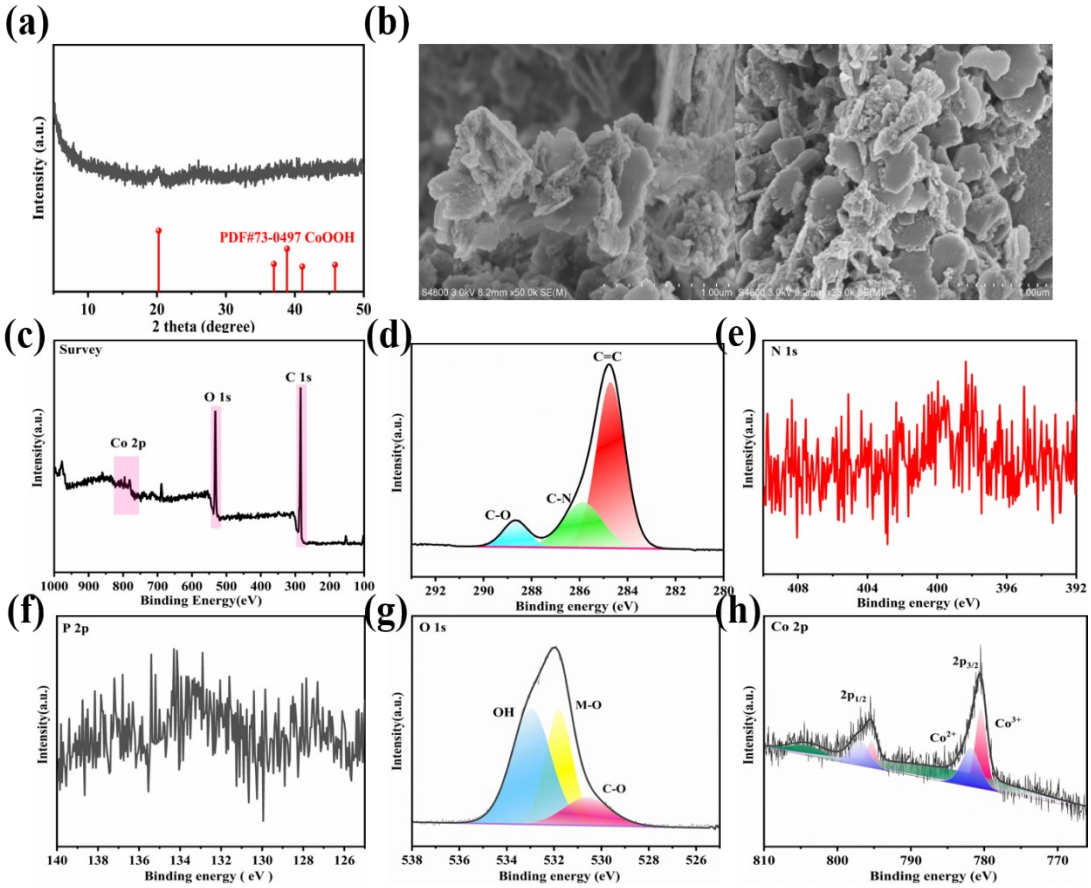

Figure. S20. XRD (a) SEM (b) and XPS (c-h) of C4NCPO-450 after 2000 CV.

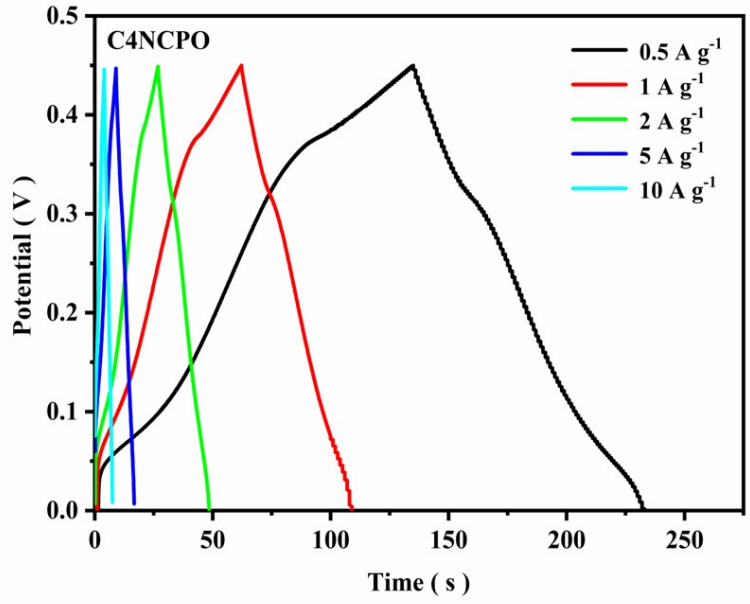

Figure. S21.The galvanostatic charge–discharge curves (GCD) at different current densities of C4NCPO.

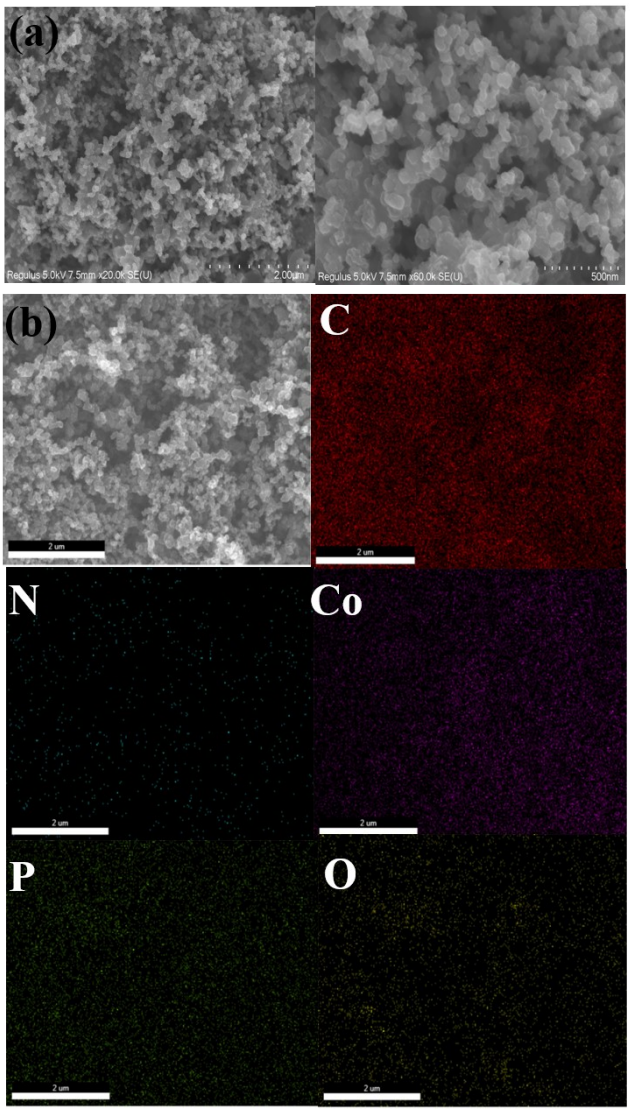

Figure S22. SEM images of CNCPO-450 after charging and discharging cycles (a) and corresponding SEM-mapping(b).

Note: In order to observe the active substance, do not add PVDF when preparing the suspension.

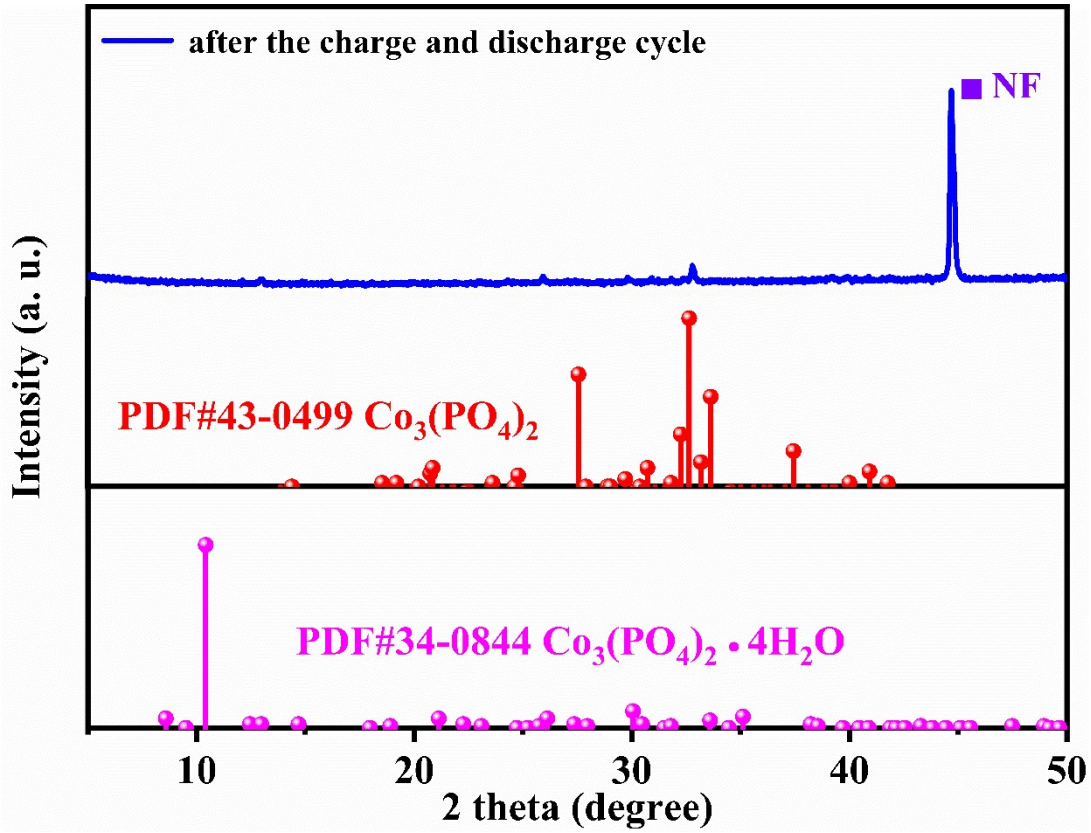

Figure S23. XRD patterns after C4NCPO-450 charge and discharge cycle.

Note: After the charge-discharge cycle test, the amorphous C4NCPO-450 showed some new peaks, which can be attributed to the cobalt phosphate species.

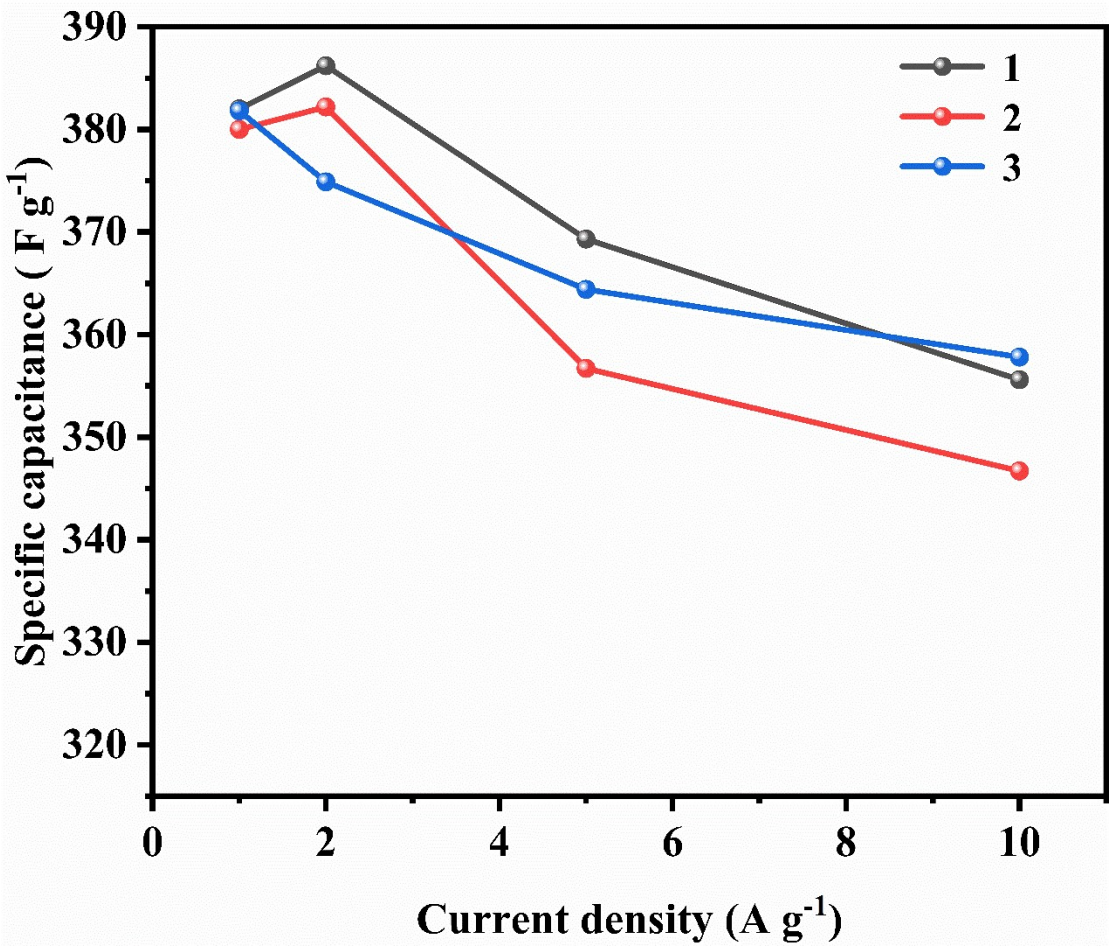

Figure S24. Three consecutive measurements of the specific capacitance of C4NCPO-450.